Computers and Chemical Engineering 125 (2019) 204–215

Contents lists available at ScienceDirect

Computers and Chemical Engineering

journal homepage: www.elsevier.com/locate/compchemeng

Operational safety of chemical processes via Safeness-Index based MPC: Two large-scale case studies

Zhihao Zhang[a], Zhe Wu[a], David Rincon[a], Carlos Garcia[a], Panagiotis D. Christofides[a,b,*]

[a] Department of Chemical and Biomolecular Engineering, University of California, Los Angeles, CA 90095-1592, USA
[b] Department of Electrical Engineering, University of California, Los Angeles, CA 90095-1592, USA

ARTICLE INFO

Article history:
Received 5 December 2018
Revised 28 February 2019
Accepted 1 March 2019
Available online 14 March 2019

Keywords:
Process safety
Operational safety
Process control
Model predictive control
Nonlinear processes

ABSTRACT

This work presents two applications of Safeness Index-based model predictive control to improve process operational safety in safety critical chemical processes. In the first case study, a high-pressure flash drum separator together with pressure relief valve as safety system is used to analyze the benefits of integrating Safeness Index-based considerations in model predictive control (MPC). In the second case study, four units in an ammonia process are simulated to demonstrate the application of Safeness Index-based MPC to handle significant disturbances.

1. Introduction

Despite efforts to prevent incidents in the chemical process industries (Center for Chemical Process Safety (2008)), the continued occurrence of accidents is motivating research focused on enhancing process operational safety to protect human lives and the environment. Several recent works have proposed a systems perspective on process operational safety (e.g., Albalawi et al. (2016); Leveson and Stephanopoulos (2014); Zhang et al. (2018)) which encourages engineers to consider process incidents as events that occur due to a migration of the process state, over time, to conditions at which an accident may occur. This systems perspective can be considered by using the optimization-based industrial feedback control design termed model predictive control (MPC), which utilizes a process dynamic model to make state predictions that are used in selecting optimal control actions with respect to an objective function (e.g., Ellis et al. (2014, 2016); Mayne et al. (2000); Rawlings (2000)). MPC can be augmented with state constraints to limit excursions of the process state into unsafe regions of state-space. Therefore, coordinating the control and safety systems so that the triggering conditions for the safety system (e.g., alarms, pressure relief devices, and emergency shutdown systems) account for control actuator limitations, and the control system actions account for the activation of the safety system, would represent a significant paradigm shift in both control and safety system design that has the potential to save lives and protect the environment. In California, there have been several accidents including one in an Exxon refinery in Torrance, Los Angeles in 2015. The total cost of this accident was estimated in more than $2.4 billion Gonzales et al. (2016). In this accident, due to malfunction of the emergency systems, major flammable vapor leaks occurred from a pipe at the fluidized catalytic cracking unit that sent thousands to the hospital; this is the type of accident that could have been prevented with coordination of the process control and emergency safety systems such that the control system could safely operate the plant in a limited operation region until the emergency system was brought back on-line (Marsh & McLennan Companies Inc (2016)).

In Mhaskar et al. (2013), Lao et al. (2013) and Bø and Johansen (2014), process control systems have been developed to handle safety in the sense of faults; however, these methods do not incorporate safety system actions in the control system design. Recently, in Albalawi et al. (2017) and Wu et al. (2018a,b), a Safeness Index function was developed to provide thresholds as triggers for safety system activation that allow the safety systems to be aware of system-level safety considerations, and further can be utilized as a constraint in MPC design to provide some coordination between control and safety systems.

In this work, we first illustrate an application of the Safeness Index-based model predictive control to improve process operational safety in a safety-critical chemical process application. A linear model is first identified from nominal process data. Then, a

* Corresponding author at: Department of Chemical and Biomolecular Engineering, University of California, Los Angeles, CA 90095-1592, USA
E-mail address: pdc@seas.ucla.edu (P.D. Christofides).

https://doi.org/10.1016/j.compchemeng.2019.03.003
0098-1354/

Safeness Index function and a Safeness Index threshold are designed to account for the key process properties and safety system characteristics. Safeness Index is integrated in MPC as a soft constraint with slack variables when the process state is outside of a safe operating region. Finally, the proposed methodology is tuned to deal with the plant/model mismatch and certain level of disturbance attenuation. The control and safety system are validated using co-simulation of Matlab/Aspen to demonstrate that Safeness Index-based MPC can either avoid activating safety system in the presence of a small disturbance, or work together with the safety system which is activated/deactivated in the presence of a large disturbance.

In the second case study, we apply the Safeness Index-based model predictive control to a multi-unit process to account for process operational safety in process control design. Specifically, the ammonia process is employed since it has been studied intensely from the last century in order to accommodate the ammonia demand. In a survey of major accidents that have occurred over a period of 70 years, the ammonia process has been ranked as the one with the greatest risk (Khan and Abbasi (1999)). Accidents and problems in the ammonia process have been reviewed in the literature Ojha and Dhiman (2010). From the simulation point of view, the effect of various types of disturbances were studied starting in the high temperature shift converter in order to avoid thermal runaway in the methanator and poison of the catalyst (Alhabdan and Elnashaie (1995)). Another type of risk in ammonia process can be associated with the following failures (Ojha and Dhiman (2010)): drop in activity of the catalyst, piping failure and oil leak. The analysis of an industrial accident that caused temperature oscillations in the ammonia synthesis reactor was studied in Morud and Skogestad (1998) and Rovaglio et al. (2004). From the control point of view, one of the first efforts on controlling the ammonia process was to obtain relevant information of the process by modeling and optimizing a large plant using first-principal models (Shah (1967); Shah and Weisenfelder (1969)). In Araújo and Skogestad (2008), a plant-wide design methodology was proposed and tested with the ammonia synthesis process. In Zhang et al. (2010), a comparison between a plant-wide control approach and a methodology that relies in simulation and heuristics was performed using the ammonia synthesis process. A framework that integrates real-time optimization with zone control MPC and self-optimization control was demonstrated in an ammonia plant in Graciano et al. (2015). Additionally, in Luyben (2012), an override control structure was implemented and simulated in Aspen Plus Dynamics to handle two types of failures in an ammonia plantwide control structure: loss of coolant in the reactor and loss of cooling water in the condenser. The closed-loop performance of the ammonia synthesis process in Luyben (2012) was improved by updating the control loops. However, at this stage, the integration between the control loop and the safety system has not been explored in the ammonia plant. Motivated by this, a dynamic simulation of parts of an ammonia plant is built in Aspen Plus software and Safeness Index-based MPC is applied to handle potential disturbances in the proposed ammonia plant process including catalyst deactivation and feed temperature change.

The rest of the paper is organized as follows: in Section 2, the process and potential failures of the first case study of a flash drum process are introduced. In Section 3, the Safeness Index function is first introduced and the Safeness Index-based MPC is then developed. In Section 4, the proposed Safeness Index-based MPC is applied to the flash drum in the presence of disturbances with different magnitudes to demonstrate its effectiveness. In Section 5, the second case study of an ammonia process is introduced. Then, in Section 6 and Section 7, the Safeness Index-based MPC is developed and applied to the multi-unit ammonia process to demonstrate that process operational safety is improved under the Safeness Index-based MPC.

2. Flash drum process description and control objective

2.1. Flash drum process description and relief valve design

As shown in Fig. 1, a flash process (Marlin (1995)) is used to roughly separate a mixture of methane (10%), ethane (20%), propane (30%), butane (35%) and pentane (5%), to a level where further distillation towers are used. A liquid feed with flow rate F, mole fraction z_i of component i, temperature T_f and pressure P_f, is heated by a heat exchanger with heating duty Q, and turned into F, z_i, T_{in}, P_{in}. Passing through a throttling valve, the feed is separated adiabatically in the drum into liquid stream L with composition x_i and vapor stream V with composition y_i. Components are separated due to different vapor pressure of different components. The feed temperature T_f is $40\,^{\circ}C$, the feed pressure P_f is $45\,bar$, the drum height is $4\,ft$ and the drum diameter is $1\,ft$.

To model a flash process, we need to apply component molar balance, energy balance, phase equilibrium and other equations, and end up with a dynamic system with state variables of drum pressure P, drum temperature T, number of moles N_i of component i in drum, mole fractions y_i and x_i of component i in vapor and liquid phase, respectively, and total number of moles N^V and N^L in vapor phase and liquid phase, respectively. Specifically, Aspen Plus Dynamics software is used to dynamically simulate this flash drum, in which the process model is built up according to the schematic in Fig. 1 and the parameters above.

In a safe scenario, controllers maintain the drum pressure near its desired value, relying on the proper operation of equipment such as pressure sensor and valves (Marlin (1995)). Two controllers are used to regulate liquid effluent valve and vapor effluent valve to maintain drum liquid level and drum pressure at desired levels, respectively. However, in an unsafe scenario where the top vapor effluent and the bottom liquid effluent valves are accidentally closed, or the broken pressure sensor causes improper control actions, an extremely high pressure will occur in the drum, which is undesired. Therefore, a pressure relief valve needs to be incorporated to handle potential dangerous situations.

Pressure relief valve is a safety device designed to protect a pressurized vessel or system in an overpressure event. In our work, Aspen Plus is used to design the pressure relief valve (e.g., size, dynamics, etc.) for this flash drum. Since the most dangerous failure situation is the vapor valve failure which normally should be directed by a controller, we design pressure relief valve parameters based on the case that the top vapor valve is totally closed accidentally due to control failure. The required relief flow is calculated as the minimum flow required to guarantee device safety, which is 523 kg/h calculated by Aspen Plus. Considering relieving conditions, fluid properties and operating conditions, a standardized orifice size of $8.303\,cm^2$ is used to meet the requirement of relief flow.

Additionally, since the operating pressure is $10\,bar$ and the highest device durable pressure is $12\,bar$, the opening pressure of the pressure relief valve is chosen to be $10.5\,bar$. Reseating pressure is set at $9\,bar$ such that the relief valve will not close once it opens until the process failure is settled. The discharge flow is considered only vapor. Flash calculation is based on constant enthalpy. The relief flow is considered compressible fluid and the discharge coefficient is 0.96.

2.2. Device failure and control objective

The flash drum initially operates at the desired operating steady-state under a model predictive controller. After operating

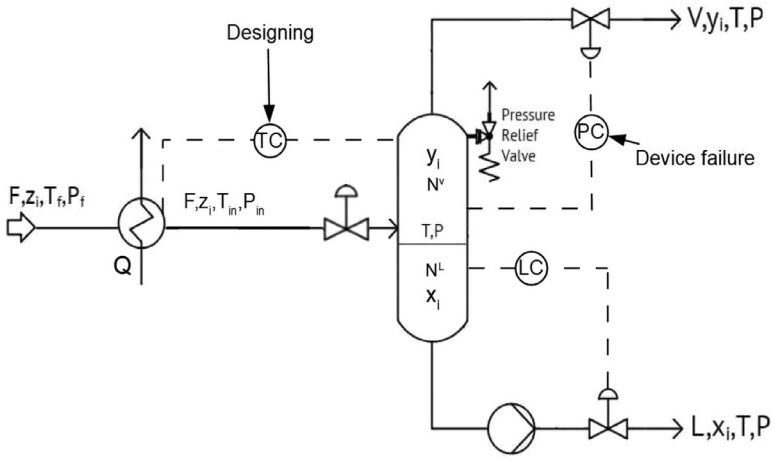

Fig. 1. A schematic of a flash process.

the drum at the steady-state, a device failure is introduced, which causes the top vapor valve to close from 50% opening to a smaller opening. As a result, the pressure P and temperature T in the drum rise up immediately, which leads to an unsafe operation.

Therefore, the objective of the control system is to maintain the drum temperature T at a desired set-point and to prevent the relief valve from opening in the presence of a small disturbance using the heating duty of the feed Q as the manipulated input. Specifically, the temperature T is controlled at the steady-state while the drum pressure P should remain below 10.5 *bar* when the top vapor valve has a failure. The worst case scenario for which we design the controller to deal with is that the top vapor valve is closed from 50% opening to 35% opening. When the top vapor valve opening is less than 35%, the pressure relief valve may open and the controller should work safely with relief valve before, during and after pressure relief valve is turned on/off (drum pressure remains less than the device maximum operating pressure of 12 *bar*).

3. Safeness index-based model predictive control

3.1. Model identification

The flash drum is simulated with high fidelity in Aspen Plus Dynamics, with a steady-state temperature and pressure $[T_s\ P_s] = [25\ ^oC\ 10\ bar]$ and a steady-state heating duty $Q_s = 87.6$ kW. The states and the input of the process are represented in deviation variable form as $x^T = [T - T_s\ P - P_s]$ and $u = Q - Q_s$, such that the equilibrium point of the system is at the origin of the state-space. Since a process model of flash drum is needed in MPC to predict future states, a linear dynamic model in the following form is identified:

$$\frac{dx}{dt} = Ax + Bu \tag{1}$$

where $A \in \mathbf{R}^{2\times 2}$ and $B \in \mathbf{R}^{2\times 1}$. We use Aspen simulation data to identify the matrices A and B in the model. Specifically, data on drum temperature T and pressure P is generated from the nominal open-loop simulations with pseudorandom binary sequence (PRBS) signal in heating duty Q. Then Multivariable Output Error State Space (MOSEP) algorithm is applied in Matlab to identify the matrices A and B as follows:

$$A = \begin{bmatrix} -0.047453 & -0.22548 \\ -0.001111 & -0.097369 \end{bmatrix}$$

$$B = \begin{bmatrix} 0.01488 \\ 0.002277 \end{bmatrix}$$

3.2. Development of safeness index

Safeness Index is a function of process state and indicates the safeness of the plant as a whole, accounting for multivariable interactions and interactions between units (Albalawi et al. (2017)). Instead of typical component-by-component safety analysis (e.g., a relief valve traditionally only accounts for pressure), Safeness Index can consider interactions between states. Moreover, a state-based index reveals that a process becomes unsafe in a gradual way (Leveson and Stephanopoulos (2014)) instead of becoming unsafe suddenly when crossing a threshold.

From fundamental process knowledge, high temperature and high pressure are the key safety issues in the flash drum. Safeness Index needs to be designed such that high temperature T and pressure P are considered unsafe operating conditions, but all the temperature T and pressure P below steady-state values are considered safe operation conditions. Therefore, in this example, Safeness Index is designed to be zero if both x_1 and x_2 are negative (e.g., below the steady-state value), and positive if either x_1 or x_2 is positive (e.g., above the steady-state value). Based on $f^+(x)$, we design the Safeness Index to be of the following form:

$$f^+(x) = \begin{cases} x, & \text{if} \quad x \geq 0 \\ 0, & \text{if} \quad x < 0 \end{cases} \tag{2}$$

$$S(x) = k_T \left[f^+\left(\frac{x_1}{T_s}\right) \right]^2 + k_P \left[f^+\left(\frac{x_2}{P_s}\right) \right]^2, \tag{3}$$

where k_T and k_P are the weights for temperature and pressure, respectively. Temperature and pressure in deviation form are divided by their steady-state values T_s and P_s for normalization such that potential difference in magnitude of the two terms are removed in the expression of the safeness index. With a quadratic form, $S(x)$ will have a significantly large value when temperature T and pressure P are far above the steady-state. Since high pressure is more dangerous than high temperature, more weight should be given to pressure P. Therefore, we choose $k_T = 1000$ and $k_P = 3000$. It is important to mention that although the Safeness Index and the Lyapunov function share similar functional forms in this case, they work to address different control objectives. Specifically, the Safeness Index is designed to indicate process safety based on measured states while the Lyapunov function is used to ensure closed-loop stability. Furthermore, the Safeness Index does not have the Lyapunov function properties. When the Safeness Index function is chosen to be a Lyapunov function, the MPC may enforce properties, such as stability and feasibility.

To avoid triggering the safety relief valve, the threshold S_{TH} of the Safeness Index function should be lower than the thresh-

old used in safety relief valve (Albalawi et al. (2017)). In consideration of model mismatch and sample-and-hold implementation of the controller, the actual threshold in the Safeness Index-based MPC needs to be more conservative to allow some overshoot in Safeness Index but not exceeding the threshold to trigger the safety relief valve. Therefore, we first calculate $S(x)$ when the relief valve is activated at 10.5 *bar* (i.e., $T = 25\ ^oC, P = 10.5$ *bar*, and $S([0\ 0.5]^T) = 7.5$). In this case, the threshold in controller is chosen as $S_{TH} = 6$.

3.3. Safeness index-based model predictive control

Safeness Index-based MPC is given by the following optimization problem:

$$\min_{u\in S(\Delta),y} \quad \int_{t_k}^{t_{k+N}} (\|\tilde{x}_1(\tau)\|_{Q_c}^2 + \|u(\tau)\|_{R_c}^2)\, d\tau + \sum_{i=1}^{N} k_1 e^{-k_2 y(i)}, \quad k_1, k_2 > 0 \tag{4a}$$

$$\text{s.t.} \quad \dot{\tilde{x}}(t) = A\tilde{x}(t) + Bu(t) \tag{4b}$$

$$\tilde{x}(t_k) = x(t_k) \tag{4c}$$

$$u(t) \in U,\ \forall\ t \in [t_k, t_{k+N}) \tag{4d}$$

$$S(\tilde{x}(t_{k+i})) + y(i) \le S_{TH},\ i = 1, 2, \ldots, N \tag{4e}$$

$$y(i) \in R,\ i = 1, 2, \ldots, N,\ if\ S(x(t_k)) > S_{TH} \tag{4f}$$

$$y(i) \ge 0,\ i = 1, 2, \ldots, N,\ if\ S(x(t_k)) \le S_{TH} \tag{4g}$$

where $\tilde{x}$ is the predicted state trajectory, $S(\Delta)$ is the set of piecewise constant functions with period Δ, and N is the number of sampling periods in the prediction horizon. The optimal input trajectory of the Safeness Index-based MPC optimization problem is $u^*(t)$, which is calculated over the entire prediction horizon $t \in [t_k, t_{k+N})$. The control action computed for the first sampling period in the prediction horizon $u^*(t_k)$ is applied over the first sampling period, and the MPC problem is resolved at the next sampling period. The objective function of Eq. (4a) is minimizing the integral of $\|\tilde{x}_1(\tau)\|_{Q_c}^2 + \|u(\tau)\|_{R_c}^2$ over the prediction horizon and the penalty term $\sum_{i=1}^{N} k_1 e^{-k_2 y(i)}$ of slack variables $y(i)$. It is noted that only state x_1 (instead of full state x) is included in the objective function because this controller is controlling only drum temperature T (pressure P is involved by Safeness Index constraints in Eq. (4e)). The constraint of Eq. (4b) is the linear model of Eq. (1) that is used to predict the states of the closed-loop system. Eq. (4c) defines the initial condition $\tilde{x}(t_k)$ of the optimization problem which is the state measurement $x(t_k)$ at $t = t_k$. Eq. (4d) is the input constraint applied over the entire prediction horizon. The manipulated input is heating duty Q, which is bounded by: $0 \le Q \le 160$ kW, namely $U = [-87.6,\ 72.4]$. Eq. (4e) is the Safeness Index constraint, which confines $S(x)$ to be below threshold S_{TH} with slack variables $y(i)$. The soft constraint of Eq. (4e) gradually affects the input when $S(x)$ gradually gets close to threshold S_{TH}, instead of causing an abrupt input if slack variables are not used. If $S(x(t_k)) > S_{TH}$, the constraint of Eq. (4e) can be satisfied via the negative slack variables $y(i)$ such that Safeness Index can remain above threshold S_{TH} in the prediction horizon, even though the penalty term $\sum_{i=1}^{N} k_1 e^{-k_2 y(i)}$ in the objective function of Eq. (4a) is large. However, if $S(x(t_k)) \le S_{TH}$, nonnegative slack variables $y(i)$ are required by Eq. (4g) to ensure $S(x)$ remaining below threshold S_{TH}. Additionally, it is demonstrated that the hard constraint of Eq. (4g) can always be satisfied in this flash drum case because of the property of A matrix in Eq. (1). Specifically, since all four elements in A matrix are negative, there always exists an input u (e.g., $u = 0$) such that $\dot{x}_1$ and $\dot{x}_2$ are simultaneously negative. Because $S(x)$ is a monotonous function with respect to x_1 and x_2, there always exists an input u such that $S(x)$ can remain below S_{TH} if $S(x(t_k)) \le S_{TH}$. Additionally, parameters k_1 and k_2 in the objective function of Eq. (4a) should be carefully chosen, such that the slack variables $y(i)$ have slight effects on control actions if $S(x(t_k)) \le S_{TH}$, and have significant effect on control actions if $S(x(t_k)) > S_{TH}$. Thus, in our simulation k_1 and k_2 are determined to be 90 and 1.6, respectively.

The explicit Euler method with an integration time step of $h_c = 10^{-3}$ s was applied to numerically integrate the dynamic model of Eq. (1) in the Safeness Index-based MPC. The nonlinear optimization problem of the Safeness Index-based MPC of Eq. (4) was solved using the solver FilterSD on OPTI Toolbox in Matlab with the following parameters: sampling period $\Delta = 0.5$ *s*; prediction horizon $N = 10$. $Q_c = 1$ and $R_c = 0.0005$ are chosen such that the terms of the states and the input have the same order of magnitude in $\|\tilde{x}_1(\tau)\|_{Q_c}^2 + \|u(\tau)\|_{R_c}^2$. Although the function $f^+(x)$ in the Safeness Index $S(x)$ in Eq. (4e) is non-differentiable at $x = 0$, the gradient of Safeness Index constraints based on f^+ in MPC is solved via numerical methods and therefore does not create difficulties in solving the optimization problem. Additionally, in this manuscript, the states in the simulations are always positive, avoiding the non-differentiable point $x = 0$.

4. Simulation results of case study 1

4.1. Simulation without safety system activation

In this section, we demonstrate the application of the Safeness Index-based MPC to a flash drum process under disturbances with different magnitudes.

When the top vapor valve is closed from 50% to 45 % opening, it is demonstrated in Figs. 2 and 3 that the pressure, temperature, and Safeness Index increase initially. As a result, the input Q is decreased by the Safeness Index-based MPC of Eq. (4) such that both $\|\tilde{x}_1(\tau)\|_{Q_c}^2$ and $\sum_{i=1}^{N} k_1 e^{-k_2 y(i)}$ in the objective function of Eq. (4a) are minimized. Specifically, $\sum_{i=1}^{N} k_1 e^{-k_2 y(i)}$ can be minimized with larger slack variables, which leads to a smaller Safeness Index over the prediction horizon and eventually leads to a decreasing input Q.

In the presence of a relatively small disturbance (e.g., the top vapor valve is closed from 50% to 45 % opening), the Safeness Index-based constraints of Eq. (4e) should not constrain process operation region too much. In other words, if $S(x(t_k)) \le S_{TH}$, small positive or zero slack variables should be utilized such that the Safeness Index is not confined to a small value according to Eq. (4e). To that end, a large k_2 in the objective function of Eq. (4a) is utilized since the term $k_1 e^{-k_2 y(i)}$ is insensitive to nonnegative slack variables $y(i)$ with a large k_2. It is observed in Fig. 3 that Safeness Index $S(x)$ finally settles down to 3.3 with $k_2 = 1.6$. However, as shown in Fig. 4, if a smaller $k_2 = 1$ is used, Safeness Index $S(x)$ will finally settle much below 3.3, which is undesired.

It needs to be mentioned that the nominal steady-state ($x = 0$) is not reached at the end of the closed-loop simulation, because the disturbance value does not go back to zero and the MPC uses

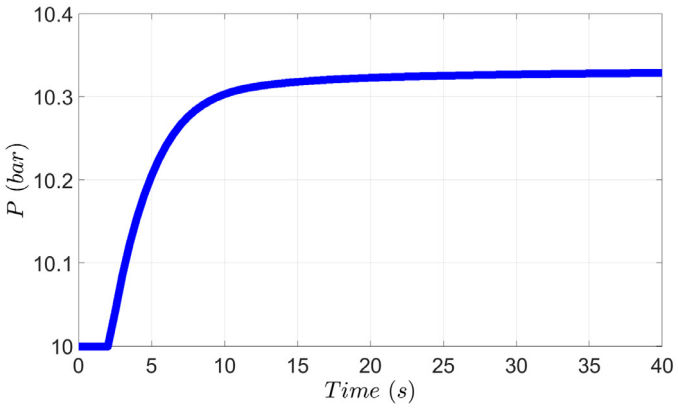

(a) Drum pressure profile

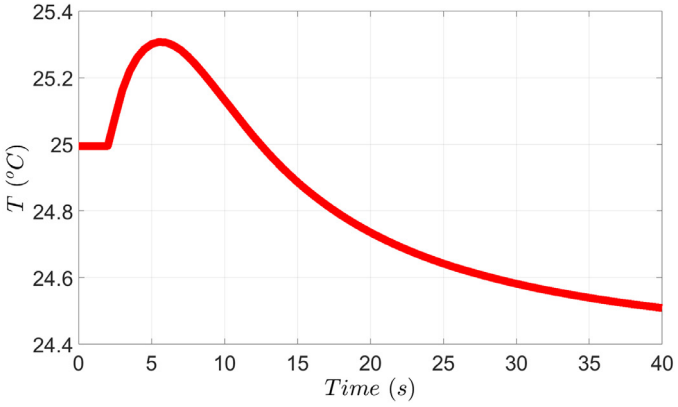

(b) Drum temperature profile

Fig. 2. Drum pressure and temperature profiles when the top vapor valve is closed from 50% to 45% opening.

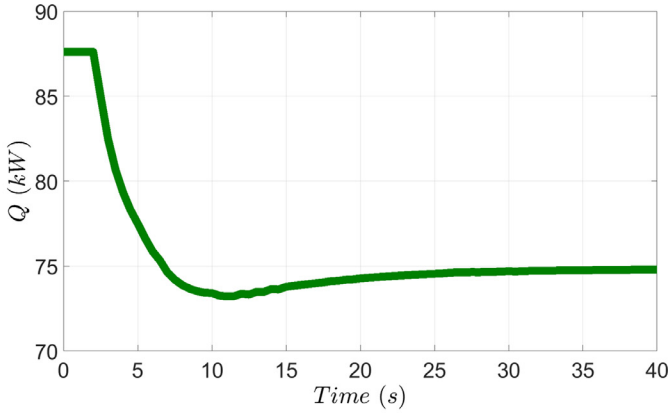

(a) Manipulated input profile

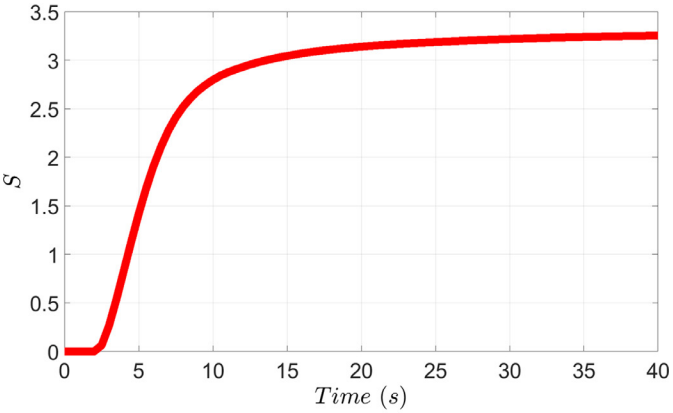

(b) Safeness Index profile

Fig. 3. Input and Safeness Index profiles when the top vapor valve is closed from 50% to 45% opening.

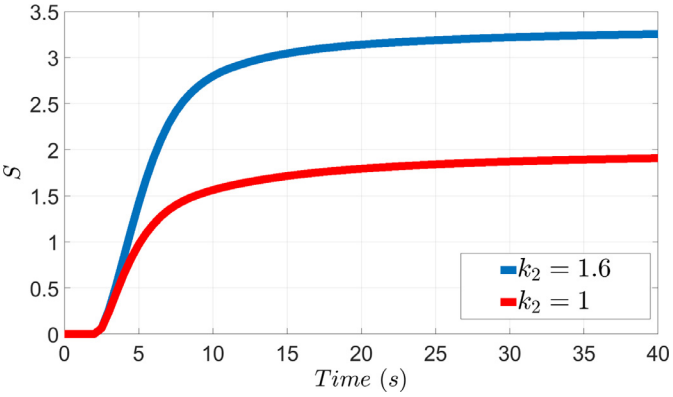

Fig. 4. Safeness Index profiles under different k_2, from which it is shown that the small k_2 (i.e., $k_2 = 1$) results in a more conservative process operation region than the large k_2 (i.e., $k_2 = 1.6$).

the nominal process model. This offset can be removed if an integral control term is added to the MPC control action but this approach is not pursued in this work.

When the top vapor valve is closed to 35% opening, it is demonstrated in Figs. 5 and 6 that the pressure, temperature and Safeness Index increase immediately after the disturbance occurs. When Safeness Index is getting close to the threshold S_{TH}, input Q becomes aggressive to prevent pressure exceeding 10.5 bar. When $S(x(t_k)) > S_{TH}$, negative positive slack variables $y(i)$ are utilized to satisfy the constraint of Eq. (4e). Since the term $\sum_{i=1}^{N} k_1 e^{-k_2 y(i)}$ dominates the objective function of Eq. (4a) when $y(i)$ are small, MPC tends to calculate relatively large slack variables $y(i)$ to decrease future Safeness Index $S(\tilde{x}(t_{k+i}))$, which leads to aggressive input Q. In Figs. 5 and 6, it is shown that the input Q decreases to its lower bound to stop Safeness Index increasing when Safeness Index is close or above the threshold S_{TH}.

Additionally, it is noted that a larger k_2 can reduce Safeness Index faster when $S(x(t_k)) > S_{TH}$. When slack variables are negative, minimizing the objective function of Eq. (4a) with larger k_2 leads to larger slack variables, which decreases Safeness Index faster by using more aggressive input. However, in the case of limited input, large k_2 is not able to decrease Safeness Index faster if the input already hits its bound when using a small k_2. As shown in Fig. 7, a large $k_2 = 2.2$ does not reduce Safeness Index S below S_{TH} because heating duty Q already reaches its minimum value even if $k_2 = 1.6$.

Additionally, model mismatch is inevitable in all simulations because the linear model of Eq. (1) used in controller is identified from the nominal system simulations, but applied to the real system with disturbance. Particularly, the disturbance dramatically increases the steady-state of temperature and pressure so that temperature and pressure increase significantly with a fixed input in the presence of disturbance. Because of model mismatch, Safeness Index based on the actual states may finally exceed the threshold S_{TH}. However, a smaller k_2 in objective function of Eq. (4a) can alleviate the adverse effect of model mismatch by calculating a conservative Safeness Index. Specifically, a small k_2 tends to calculate larger slack variables if slack variables are positive. It is demonstrated in Eq. (4e) that larger slack variables lead to a lower and conservative Safeness Index, which can bring Safeness Index to a lower value to alleviate the adverse effect of model mismatch.

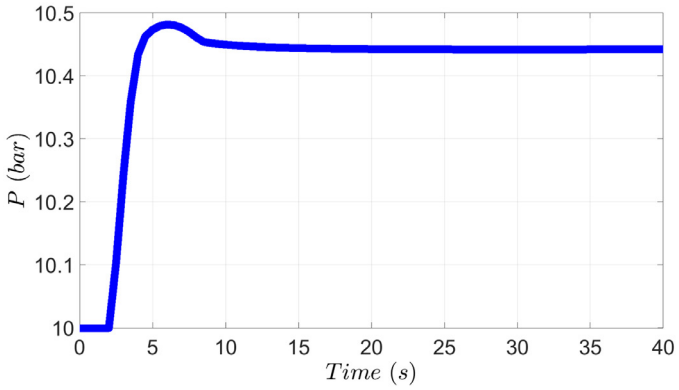

(a) Drum pressure profile

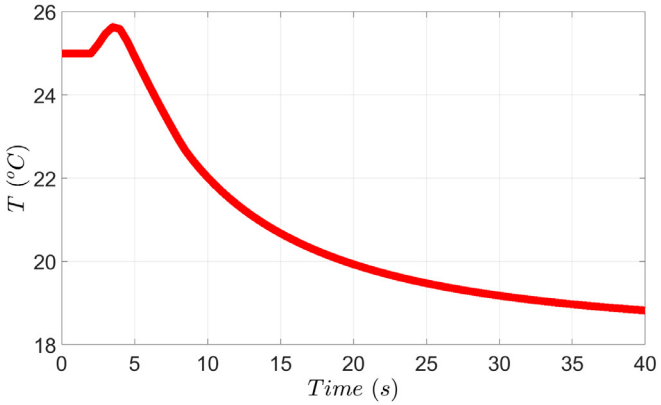

(b) Drum temperature profile

Fig. 5. Drum pressure and temperature profiles when the top vapor valve is closed from 50% to 35% opening.

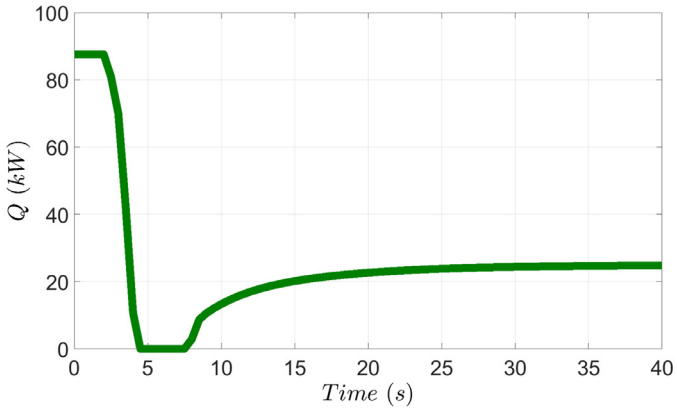

(a) Manipulated input profile

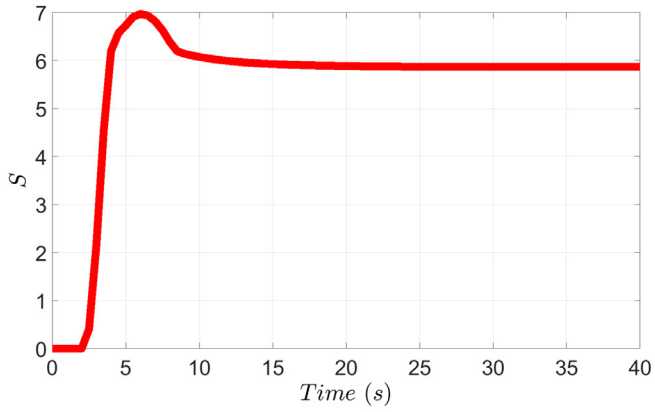

(b) Safeness Index profile

Fig. 6. Input and Safeness Index profiles when the top vapor valve is closed from 50% to 35% opening.

Additionally, parameters k_1 and k_2 should be well-determined to account for how conservative the threshold S_{TH} is compared to the threshold of safety system. If the threshold S_{TH} is very conservative, a large k_2 is preferred such that the Safeness Index can keep close to the threshold S_{TH} under all disturbances. If the threshold S_{TH} is not conservative, a small k_2 is preferred so that the Safeness Index can remain below the threshold S_{TH}. Parameter k_1 should be chosen according to k_2 so that the term $\int_{t_k}^{t_{k+N}}(\|\tilde{x}_1(\tau)\|_{Q_c}^2 + \|u(\tau)\|_{R_c}^2)\,d\tau$ in the objective function of Eq. (4a) is larger than the term $\sum_{i=1}^{N} k_1 e^{-k_2 y(i)}$ under a relatively small disturbance, and smaller under a large but handleable disturbance.

4.2. Simulation with safety system activation

In the presence of a very large disturbance, the control system is unable to prevent a high pressure inside the drum due to actuator constraints. In this simulation, the top vapor valve is changed from 50% opening to 10% opening. As shown in Figs. 8 and 9, the drum pressure P rises above 10.5 bar even when the minimum heating duty Q is provided. Then, the pressure relief valve is activated to allow the pressurized fluid to flow out of the drum. MPC drives the temperature T to 0.2 ^oC below the set-point (25 ^oC) because of model mismatch from vapor valve disturbance and relief valve opening. After 40 s, the device failure is fixed and the top vapor valve returns to 50% opening. Then the pressure P decreases immediately after opening the vapor valve. When the pressure P decreases to 9 bar which is the reseating pressure, the safety relief valve is closed and the process states are driven to the steady-state by the Safeness Index-based MPC.

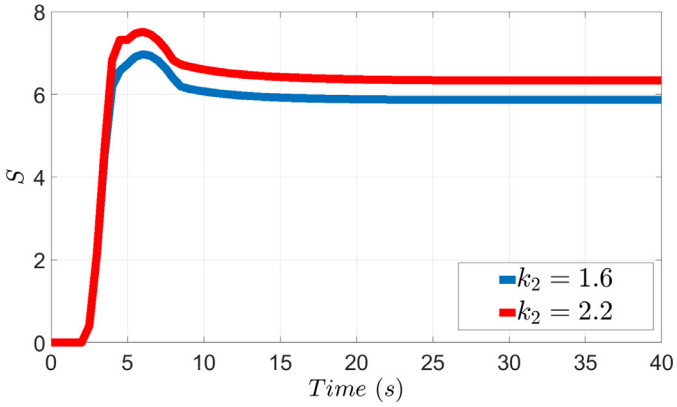

Fig. 7. Safeness Index profiles under different k_2, from which it is shown that the large k_2 (i.e., $k_2 = 2.2$) does not reduce Safeness Index S below S_{TH}.

5. Ammonia process description

The second case study focuses on three parts of ammonia process: shift conversion, carbon dioxide removal and methanation. As shown in Fig. 10, all the three parts are used to remove carbon monoxide and carbon dioxide, which are produced by the previous steam reformer. The schematic of the ammonia process implemented in this manuscript is shown in Fig. 11.

First, the high temperature shift reactor and the low temperature shift reactor are two adiabatic tubular reactors, converting carbon monoxide and water into carbon dioxide and hydrogen. Two-bed operation is performed in which different catalyst are utilized

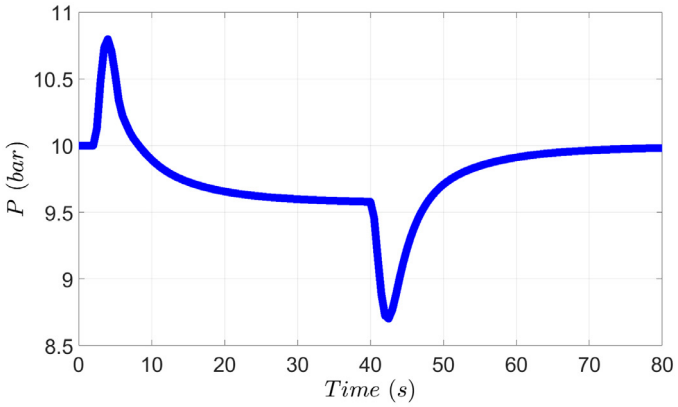

(a) Drum pressure profile

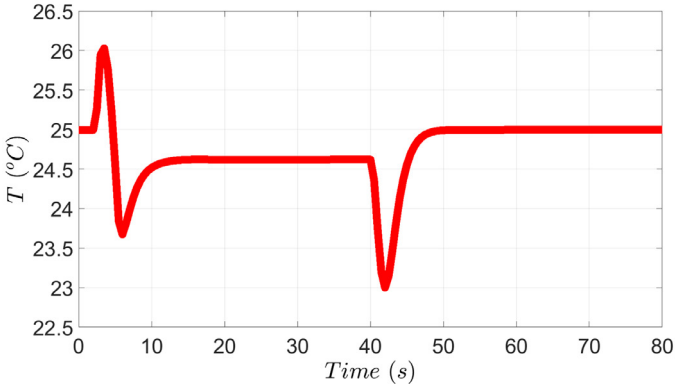

(b) Drum temperature profile

Fig. 8. Drum pressure and temperature profiles when the top vapor valve is closed from 50% to 10% opening.

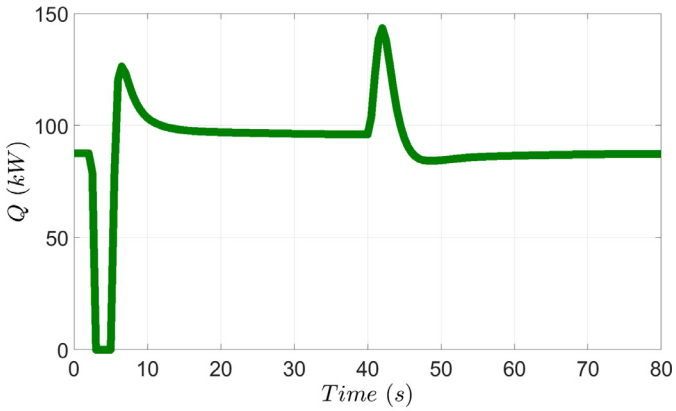

(a) Manipulated input profile

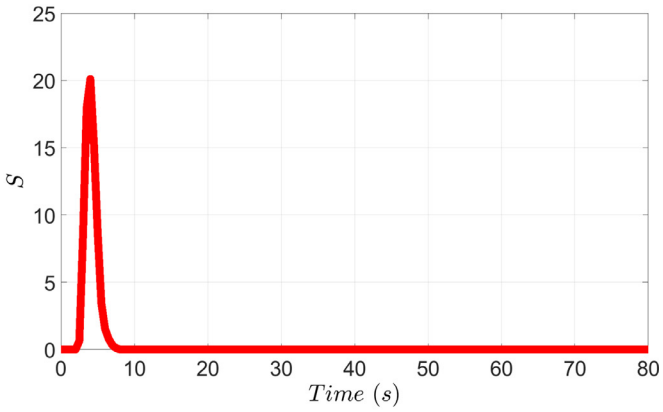

(b) Safeness Index profile

Fig. 9. Input and Safeness Index profiles when the top vapor valve is closed from 50% to 10% opening.

in each bed that is operated at different temperatures, typically at 400 °C and 200 °C, respectively. Under normal operating conditions, the high temperature shift reactor is able to reduce the carbon monoxide to 2 – 4 %, and the low temperature shift reactor can obtain an output of carbon monoxide between 0.1 – 0.3 % (Appl (2000); Ettouney et al. (1995); Twigg (1989)).

After two shift reactors, the gas is purified in the adsorption column to remove the carbon dioxide and water vapor, in order to avoid the poison of the ammonia synthesis catalysts (Appl (2000)).

After removal unit, methanation unit is applied to remove trace amount of carbon monoxide and carbon dioxide since even a small amount of carbon monoxide and carbon dioxide in syn-gas is poisonous to ammonia synthesis catalysts. In the methanator, the concentrations of carbon monoxide and carbon dioxide are reduced to less than 5 ppm catalytically by exothermic methanation reaction (Ojha and Dhiman (2010); Twigg (1989)).

5.1. Simulation settings in Aspen Plus

In our study, the simulations of all the ammonia process units are performed in Aspen plus and Aspen plus Dynamics V10.0. A dynamic simulation is developed based on the steady-state simulation provided by Aspen Technology, Inc. (2017). Detailed reaction kinetic and process parameters are discussed in this section. Specifically, reaction rates for all reactions are incorporated in Aspen Plus model via the compiling and linking of the FORTRAN file with Aspen Plus software. The rate equations for all units are shown as following (Aspen Technology, Inc. (2017); Ettouney et al. (1995)):

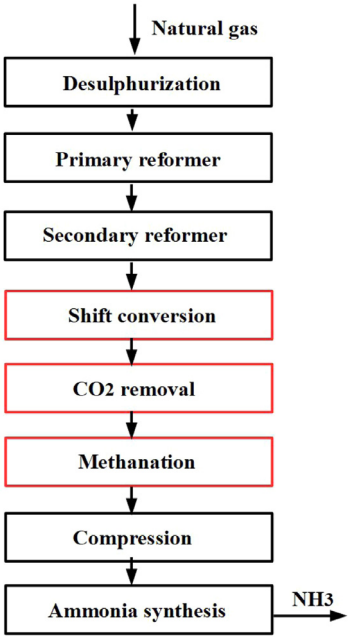

Fig. 10. A schematic of an ammonia process.

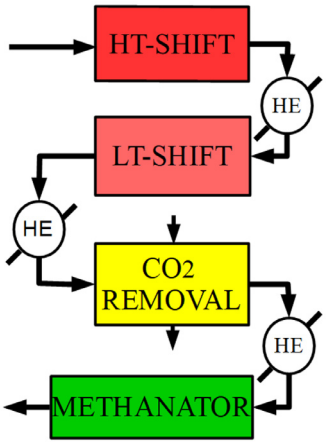

Fig. 11. A schematic of all simulated units in this manuscript, where HT-SHIFT, HE, LT-SHIFT, CO_2 REMOVAL and METHANATOR represent the high temperature shift reactor, heat exchanger, low temperature shift reactor, CO_2 removal and methanator, respectively.

High temperature shift reaction: $CO + H_2O \rightleftarrows CO_2 + H_2$, $\Delta H = -41.2$ kJ/mol:

$$r_{CO} = -A_c \exp\left(-\frac{300.69}{T} + 8.02\right)(P)^{1/2}\left(y_{CO} - \frac{y_{H_2} y_{CO_2}}{K_{eq} y_{H_2O}}\right),$$
$$K_{eq} = \exp\left(\frac{8240}{T} - 4.33\right) \tag{5}$$

Low temperature shift reaction: $CO + H_2O \rightleftarrows CO_2 + H_2$, $\Delta H = -41.2$ kJ/mol:

$$r_{CO} = -A_c \frac{513.15}{T} \frac{K_L y_{CO} y_{H_2O}^{1/2}\left(1 - \frac{K}{K_{eq}}\right)}{\frac{1}{P} + K_A y_{CO} + K_B y_{CO_2}}, \quad K = \frac{y_{H_2} y_{CO_2}}{y_{CO} y_{H_2O}},$$
$$K_{eq} = \exp\left(\frac{8240}{T} - 4.33\right),$$
$$K_L = 68.4 \exp\left(-3620\left(\frac{1}{513.15} - \frac{1}{T}\right)\right),$$
$$K_A = 4.31 \exp\left(-4580\left(\frac{1}{513.15} - \frac{1}{T}\right)\right),$$
$$K_B = 1.35 \exp\left(-1500\left(\frac{1}{513.15} - \frac{1}{T}\right)\right) \tag{6}$$

Methanation reaction 1: $CO + 3H_2 \rightleftarrows CH_4 + H_2O$, $\Delta H = -206$ kJ/mol:

$$r_{CO} = -A_c\ 3.119\ exp\left(1300\left(\frac{1}{T} - \frac{1}{513}\right)\right)\left(\frac{P}{y_{H_2}}\right)^{1/2} \times\left(y_{CO} - \frac{y_{CH_4}\ y_{H_2O}}{y_{H_2}^3\ P^2\ exp\left(-38.4523 + \frac{2627}{T}\right)}\right) \tag{7}$$

Methanation reaction 2: $CO_2 + 4H_2 \rightleftarrows CH_4 + 2H_2O$, $\Delta H = -164$ kJ/mol:

$$r_{CO} = -A_c\ 3.119\ exp\left(1300\left(\frac{1}{T} - \frac{1}{513}\right)\right)\left(\frac{P}{y_{H_2}}\right)^{1/2} \times\left(y_{CO_2} - \frac{y_{CH_4}\ y_{H_2O}^2}{y_{H_2}^4\ P^2\ exp\left(-38.4523 + \frac{2627}{T}\right)}\right) \tag{8}$$

where r_{CO} is the reaction rate of CO in gmol/m$^3 \cdot s$; A_c is catalyst activity; T is the temperature in K; P is the total pressure in atm; and y_i is the mole fraction of component i.

In our simulation, all heat exchangers work at the fixed outlet temperature with varying heating duty. All three tube reactors are adiabatic in this simulation. CO_2 removal unit is simulated as a flash drum at 30 °C with feeding ammonia solution to remove CO_2 and condense water. Detailed electrolyte solution chemistry and reaction kinetic in CO_2 removal is discussed in Aspen Technology, Inc. (2017). The values of the main parameters and their steady-states are shown in Table 1.

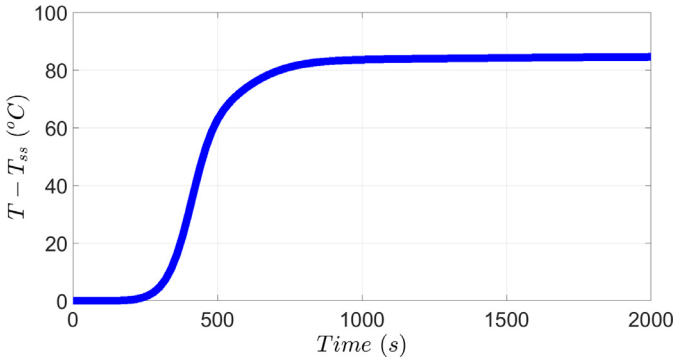

Fig. 12. Methanator outlet temperature profile, from which it is shown that $T - T_{ss}$ increases more than 80 °C after the catalyst activity in high temperature shift reactor decreases from 1 to 0.1 in 300 s.

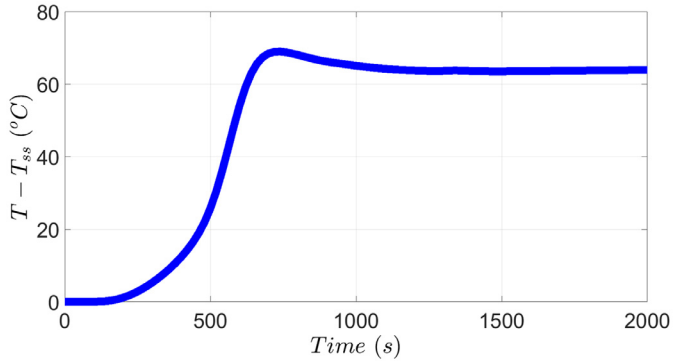

Fig. 13. Methanator outlet temperature profile, from which it is shown that $T - T_{ss}$ increases more than 60 °C after the feed temperature of high temperature shift reactor decreases from 380 °C to 280 °C in 300 s.

5.2. Disturbance and process safety

Initially, all units are operated at the steady-states. When catalyst activity decreases in the first high temperature shift reactor, less CO is consumed in the shift reactor. Since CO_2 removal unit does not remove CO, more CO goes into methanator, which leads to a drastic increase in temperature due to the exothermic reaction of methanation occurred in the adiabatic tube reactor. Fig. 12 shows an open-loop simulation with a disturbance that catalyst activity decreases from 1 to 0.1 in 300 s.

On the other hand, when feed temperature decreases in the first high temperature shift reactor, less CO is reacted in shift reactor. Similarly, since CO_2 removal unit does not remove CO, more CO goes into methanator and causes the temperature in methanator to increase drastically. Fig. 13 shows an open-loop simulation with a disturbance that feed temperature for high temperature shift reactor decreases from 380 °C to 280 °C in 300 s. Therefore, in order to improve process operational safety in the presence of these two types of disturbances, a controller is designed to control methanator outlet temperature by manipulating methanator inlet feed temperature.

Table 1
Parameter values of the ammonia process simulation.

Feed	Temperature 980 °C Mole fraction y_{CO_2} 0.0507	Pressure 29 *bar* Mole fraction y_{H_2} 0.355	Molar flowrate 3435 *mol/s* Mole fraction y_{H_2O} 0.353	Mole fraction y_{CO} 0.0839 Mole fraction y_{N_2} 0.152
HT-shift	Reactor length 15.8 *m* Catalyst heat capacity 900 *J/kg K*	Reactor diameter 4.4 *m* Feed temperature 360 °C	Loaded catalyst 9.61×10^4 *kg*	Voidage 0.5
LT-shift	Reactor length 7.7 *m* Catalyst heat capacity 850 *J/kg K*	Reactor diameter 3.7 *m* Feed temperature 210 °C	Loaded catalyst 3.48×10^4 *kg*	Voidage 0.5
CO_2 Removal	Volume 49.09 m^3 H_2O removal rate 99.7%	Temperature 30 °C	Pressure 26.9 *bar*	CO_2 removal rate 98.6%
Methanator	Reactor length 4 *m* Catalyst heat capacity 900 *J/kg K*	Reactor diameter 2.5 *m* Feed temperature 280 °C	Loaded catalyst 1.57×10^4 *kg*	Voidage 0.5

6. Safeness index-based model predictive control

6.1. Model identification

The methanator is initially simulated at the steady-state where feed temperature $T_{in} = 280\,^{\circ}C$ and outlet temperature $T_{out} = 327.27\,^{\circ}C$. Because CO concentration in the feed has a dominating effect on the produced heat, CO mole fraction y_{CO} is treated as a measurable disturbance with a steady-state value of 3.55×10^{-3}. The state, the input and the disturbance of the process are represented in deviation variable form as $x = T_{out} - T_{out,ss}$, $u = T_{in} - T_{in,ss}$ and $d = y_{CO} - y_{CO,ss}$, such that the equilibrium point of the system is at zero. Since there exists a time delay between the feed temperature T_{in} and the outlet temperature T_{out}, a linear dynamic model with time delay of the following form is utilized to represent the Aspen Plus model:

$$\frac{dx(t)}{dt} = Ax(t) + Bu(t - t_d) + Kd(t - t_d), \tag{9}$$

where t_d is the time delay in s. It is noted that the input time delay is equal to the disturbance time delay because it takes the same amount of time for the feed temperature T_{in} and the CO mole fraction of y_{CO} to affect the outlet temperature T_{out} of a tube reactor. An Aspen open-loop simulation is used to generate transient response data of outlet temperature T_{out} subject to a step change in feed temperature T_{in}, and Multivariable Output Error State Space (MOSEP) algorithm is applied in Matlab to identify the matrices A and B. Then another step change in CO mole fraction of y_{CO} is simulated to calculate the gain K of disturbance d. The difference among the models obtained from the different step changes are negligible. The matrices A, B, K and the time delay t_d are identified as follows:

$$A = -0.005136; \quad B = 0.01207; \quad K = 32.887; \quad t_d = 100\ s$$

6.2. Safeness index and controller design

Since temperature control plays an important role in the methanator, and high outlet temperature could lead to unsafe operations, in our work Safeness Index is designed such that high temperature T_{out} is considered unsafe operating conditions while all the temperature T_{out} below steady-state values are considered safe operation conditions. To that end, Safeness Index is design as follows:

$$S(x) = [f^+(x)]^2, \tag{10}$$

where $f^+(x)$ is the same function as shown in Eq. (2). With a quadratic form, $S(x)$ will have a significantly large value when temperature T_{out} is far above the steady-state. To avoid an extreme high temperature in methanator, the threshold S_{TH} of the Safeness Index function $S(x)$ is carefully chosen. In consideration of model mismatch, sample-and-hold implementation of the controller and the large time delay in the process, the actual threshold in the Safeness Index-based MPC should be more conservative and therefore is chosen to be $S_{TH} = 5^2 = 25$. Based on the Safeness Index function of Eq. (10), the controller is developed by incorporating MPC with a feedforward control action as shown in Eq. (11):

$$u(t_k) = u_{MPC}(t_k) + u_{forward}(t_k) \tag{11}$$

Specifically, the control action $u(t_k)$ consists of a feedforward term $u_{forward}(t_k)$ and an MPC term $u_{MPC}(t_k)$, where $u_{forward}(t_k)$ is calculated by Eq. (12) and $u_{MPC}(t_k)$ is the first control action in the solution $u^*(t)$ to the optimization problem of Eq. (13).

$$u_{forward}(t_k) = -\frac{K}{B} d(t_k) \tag{12}$$

$$\min_{u \in S(\Delta), y} \quad \int_{t_k + t_d}^{t_{k+N} + t_d} (\|\tilde{x}(\tau)\|_{Q_c}^2)\ d\tau + \int_{t_k}^{t_{k+N}} (\|u(\tau)\|_{R_c}^2)\ d\tau + \sum_{i=1}^{N} k_1 e^{-k_2 y(i)}, \quad k_1, k_2 > 0 \tag{13a}$$

$$\text{s.t.} \quad \dot{\tilde{x}}(t) = A\tilde{x}(t) + Bu(t - t_d) \tag{13b}$$

$$\tilde{x}(t_k) = x(t_k) \tag{13c}$$

$$u(t) = u_{pre}(t), \ \forall\ t \in [t_k - t_d, t_k) \tag{13d}$$

$$u(t) \in U, \ \forall\ t \in [t_k, t_{k+N}) \tag{13e}$$

$$S(\tilde{x}(t_{k+i} + t_d)) + y(i) \le S_{TH}, \ i = 1, 2, \ldots, N \tag{13f}$$

$$y(i) \ge 0, \ i = 1, 2, \ldots, N,$$

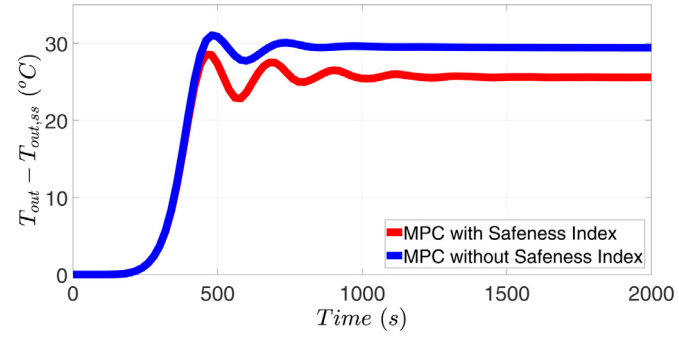

(a) Methanator outlet temperature profile

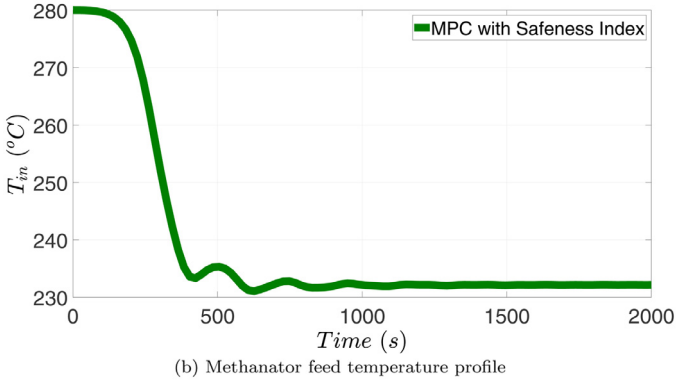

(b) Methanator feed temperature profile

Fig. 14. Close-loop simulation results when the catalyst activity in the high temperature shift reactor decreases from 1 to 0.1 in 300 *s*.

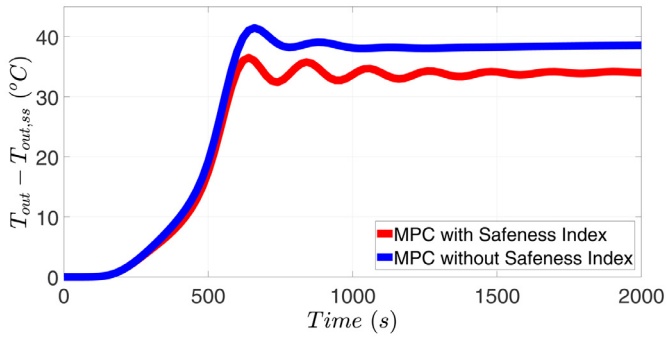

(a) Methanator outlet temperature profile

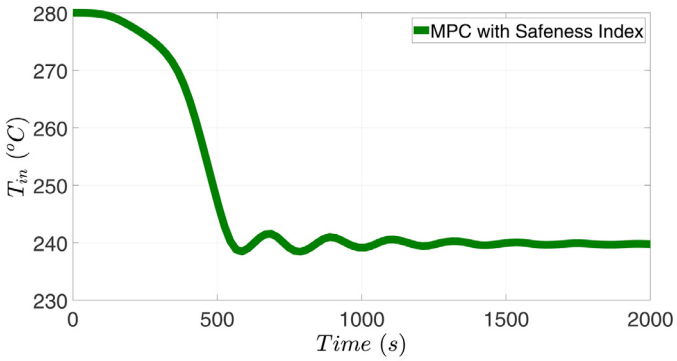

(b) Methanator feed temperature profile

Fig. 15. Close-loop simulation results when the feed temperature of the high temperature shift reactor decreases from 380 °*C* to 280 °*C* in 300 *s*.

$$if\ S(\tilde{x}(t_k + t_d)) \le S_{TH} \tag{13g}$$

$$y(i) \in R,\ \ i = 1, 2, \ldots, N,$$
$$if\ S(\tilde{x}(t_k + t_d)) > S_{TH} \tag{13h}$$

where the notation follows that in Eq. (4). Although the optimal input trajectory $u^*(t)$ is calculated over the entire prediction horizon $t \in [t_k,\ t_{k+N})$, the control action computed for the first sampling period in the prediction horizon $u(t_k)$ is applied over the first sampling period, and the MPC problem is resolved at the next sampling period. The objective function of Eq. (13a) is minimizing the integral term $\int_{t_k+t_d}^{t_{k+N}+t_d}(\|\tilde{x}(\tau)\|^2_{Q_c})\ d\tau$ and $\int_{t_k}^{t_{k+N}}(\|u(\tau)\|^2_{R_c})\ d\tau$ and the penalty term $\sum_{i=1}^{N} k_1 e^{-k_2 y(i)}$ of slack variables $y(i)$. It is noted that state is integrated from $t_k + t_d$ to $t_{k+N} + t_d$ because state from t_k to $t_k + t_d$ is already determined by previous implemented control actions. The constraint of Eq. (13b) is the nominal linear model of Eq. (9) that is used to predict the states of the closed-loop system. Because the disturbance is mitigated by the feedforward term (i.e., $u_{forward}(t_k)$), MPC utilizes the nominal system of Eq. (13b) for prediction. Eq. (13c) defines the initial condition $\tilde{x}(t_k)$ of the optimization problem which is the state measurement $x(t_k)$ at $t = t_k$. Eq. (13d) provides input trajectory calculated from previous steps, in order to predict state from t_k to $t_k + t_d$. Eq. (13e) is the input constraint applied over the entire prediction horizon. The manipulated input is the feed temperature T_{in}, which is bounded by: $180\,^\circ C \le T_{in} \le 380\,^\circ C$, namely $U = [-100,\ \ 100]$. Eq. (13f) is the Safeness index constraints with slack variables $y(i)$. If $S(x(t_k + t_d)) > S_{TH}$, the constraint of Eq. (13f) can be satisfied via the negative slack variables $y(i)$ such that Safeness Index can remain above threshold S_{TH} in the prediction horizon. However, if $S(x(t_k)) \le S_{TH}$, nonnegative slack variables $y(i)$ are required by Eq. (13g) to ensure $S(x)$ remaining below threshold S_{TH}. Additionally, parameters k_1 and k_2 in the objective function Eq. (13a) should be carefully chosen, such that the slack variables $y(i)$ have slight effects on control actions if $S(x(t_k + t_d))$ is far below S_{TH}, and have significant effects on control actions if $S(x(t_k + t_d))$ is close to S_{TH}. Thus, in our simulation k_1 and k_2 are determined to be 10^5 and 0.2, respectively.

The explicit Euler method with an integration time step of $h_c = 10^{-1}$ s was applied to numerically integrate the dynamic model of Eq. (9) in Safeness Index-based MPC. The nonlinear optimization problem of Safeness Index-based MPC of Eq. (13) was solved using the solver FilterSD on OPTI Toolbox in Matlab with the following parameters: sampling period $\Delta = 20$ s; prediction horizon $N = 30$. $Q_c = 1$ and $R_c = 0.5$ are chosen such that the terms of the states and the input have the same order of magnitude in $\|\tilde{x}_1(\tau)\|^2_{Q_c}$ and $\|u(\tau)\|^2_{R_c}$.

7. Simulation results of case study 2

In this section, we demonstrate the application of the proposed controller to the ammonia process in the presence of different disturbances.

7.1. Disturbance 1: catalyst activity

After the catalyst activity in the high temperature shift reactor decreases from 1 to 0.1 in 300 *s*, less *CO* is reacted in the high temperature shift reactor. Although the low temperature shift reactor buffers the increasing *CO* content, a higher concentration of *CO* still reaches the methanator and causes an increasing temperature. The *CO* mole fraction y_{CO} in the feed of methanator is measured at each sampling time t_k and sent to the feedforward controller at time t_k to account for the effect of disturbance. However, it is noted that since *CO* is not the only disturbance to the methanator due to catalyst deactivation, this feedforward term is not able to mitigate all the disturbances. Moreover, model mismatch still exists between the identified linear model and the actual process. As

a result, the outlet temperature of the methanator increases after the disturbance is introduced and does not go back to the origin.

Fig. 14 shows that the outlet temperature of methanator T_{out} can increase more than $30\,^{\circ}C$ if the Safeness Index constraints are not utilized in MPC, while it increases less than $30\,^{\circ}C$ if Safeness Index constraints are utilized in MPC, which implies that the Safeness Index-based MPC can improve process operational safety of the ammonia plant.

7.2. Disturbance 2: feed temperature

After the feed temperature in the high temperature shift reactor decreases from $380\,^{\circ}C$ to $280\,^{\circ}C$, the temperature in the high temperature shift reactor starts to decrease slowly since it takes some time for a large amount of catalyst to cool down. As a result, the CO mole fraction y_{CO} in the feed of methanator increases gradually, and the temperature in methanator increases but slower than the case of disturbance 1.

Fig. 15 shows that the outlet temperature of methanator T_{out} can increase more than $40\,^{\circ}C$ if the Safeness Index constraints are not utilized in MPC, while it increases less than $40\,^{\circ}C$ if the Safeness Index constraints are utilized in MPC. On the other hand, by comparing Figs. 15 and 14, it is demonstrated that the temperature increases more with less control actions (i.e., lower inlet temperature) in the presence of disturbance 2. The reason is that the CO concentration in the feed to the methanator is much less under disturbance 2 than under disturbance 1, which leads to a significantly small feedforward control action $u_{forward}$ in the presence of disturbance 2. Therefore, even though u_{MPC} is calculated to be larger in the case of disturbance 2 since the outlet temperature is further away from the steady state compared to disturbance 1, the overall control action calculated from $u = u_{MPC} + u_{forward}$ under disturbance 2 is still less than the one under disturbance 1.

It needs to be mentioned that the closed-loop state has an offset under both disturbances. Although a feedforward term is added to compensate for the measured disturbance, not all process disturbances can be measured in a multi-unit process. In future work, further offset-free feature may be implemented in MPC as discussed in Wallace et al. (2016).

8. Conclusion

This work demonstrated two applications of Safeness Index-based model predictive control to improve process operational safety in safety critical chemical processes. In the first case study, a high-pressure flash drum separator together with pressure relief valve as safety system was utilized to analyze the benefits of integrating Safeness Index-based considerations in model predictive control (MPC). Specifically, a Safeness Index function and a Safeness Index threshold were developed using information collected from the process and safety system to indicate the safeness of the plant. Then, under an identified linear model, MPC was implemented with Safeness Index-based constraints and slack variables in a co-simulation of Matlab/Aspen. It was demonstrated that in the presence of a small disturbance, the drum pressure remains below the opening pressure of relief valve by Safeness Index-based MPC such that the safety system was not activated. However, in the presence of a large disturbance, the controller working together with the relief valve ensured process operational safety before, during and after the pressure relief valve was turned on/off.

In the second case study, four units in the ammonia process were simulated to demonstrate the application of Safeness Index. To ensure process operational safety in the presence of a significant propagated disturbance to methanation unit in the ammonia process, a Safeness Index function and a Safeness Index threshold were developed to characterize the safeness of an adiabatic methanation tube reactor. Subsequently, a linear dynamic model with time delay and disturbance were identified for the methanator. Finally, an MPC was developed with the Safeness Index-based constraints and feedforward disturbance compensation term to improve the performance of MPC and to handle the propagated disturbance.

Acknowledgments

Financial support from the National Science Foundation and the Department of Energy is gratefully acknowledged.

Supplementary material

Supplementary material associated with this article can be found, in the online version, at doi:10.1016/j.compchemeng.2019.03.003.

References

Albalawi, F., Alanqar, A., Durand, H., Christofides, P.D., 2016. A feedback control framework for safe and economically-optimal operation of nonlinear processes. AIChE J. 62, 2391–2409.
Albalawi, F., Durand, H., Christofides, P.D., 2017. Process operational safety using model predictive control based on a process safeness index. Comput. Chem. Eng. 104, 76–88.
Alhabdan, F., Elnashaie, S., 1995. Simulation of an ammonia plant accident using rigorous heterogeneous models: effect of shift converters disturbances on the methanator. Math. Comput. Model. 21, 85–106.
Appl, M., 2000. Ammonia. Ullmann's Encyclopedia of Industrial Chemistry. Wiley – VCH Verlag GmbH & Co. KGaA.
Araújo, A., Skogestad, S., 2008. Control structure design for the ammonia synthesis process. Comput. Chem. Eng. 32, 2920–2932.
Aspen Technology, Inc., 2017. Aspen Plus ammonia model. Bedford, MA.
Bø, T.I., Johansen, T.A., 2014. Dynamic safety constraints by scenario based economic model predictive control. In: Proceedings of the IFAC World Congress. Cape Town, South Africa, pp. 9412–9418.
Center for Chemical Process Safety, 2008. Guidelines for Hazard Evaluation Procedures. John Wiley & Sons, Inc., Hoboken, New Jersey. third edition.
Ellis, M., Durand, H., Christofides, P.D., 2014. A tutorial review of economic model predictive control methods. J. Process Control 24, 1156–1178.
Ellis, M., Liu, J., Christofides, P.D., 2016. Economic Model Predictive Control: Theory, Formulations and Chemical Process Applications. Springer, London, England.
Ettouney, H.M., Shaban, H.I., Nayfeh, L.J., 1995. Theoretical analysis of high and low temperature shift converters. Chem. Eng. Commun. 134, 1–16.
Gonzales, D., Gulden, T.R., Strong, A., Hoyle, W., 2016. Cost-Benefit Analysis of Proposed California Oil and Gas Refinery Regulations. Rand Corporation.
Graciano, J.E.A., Jäschke, J., Le Roux, G.A., Biegler, L.T., 2015. Integrating self-optimizing control and real-time optimization using zone control MPC. J. Process Control 34, 35–48.
Marsh & McLennan Companies Inc, 2016. The 100 Largest Losses 1974–2015: Large Property Damage Losses in the Hydrocarbon Industry. Technical Report. Marsh & McLennan Companies Inc.
Khan, F.I., Abbasi, S.A., 1999. Major accidents in process industries and an analysis of causes and consequences. J. Loss Prev. Process Ind. 12, 361–378.
Lao, L., Ellis, M., Christofides, P.D., 2013. Proactive fault-tolerant model predictive control. AIChE J. 59, 2810–2820.
Leveson, N.G., Stephanopoulos, G., 2014. A system-theoretic, control-inspired view and approach to process safety. AIChE J. 60, 2–14.
Luyben, W.L., 2012. Use of dynamic simulation for reactor safety analysis. Comput. Chem. Eng. 40, 97–109.
Marlin, T., 1995. Process Control: Designing Process and Control Systems for Dynamic Performance. McGraw-Hill, New York.
Mayne, D.Q., Rawlings, J.B., Rao, C.V., Scokaert, P.O.M., 2000. Constrained model predictive control: stability and optimality. Automatica 36, 789–814.
Mhaskar, P., Liu, J., Christofides, P.D., 2013. Fault-Tolerant Process Control: Methods and Applications. Springer-Verlag, London, England.
Morud, J.C., Skogestad, S., 1998. Analysis of instability in an industrial ammonia reactor. AIChE J. 44, 888–895.
Ojha, M., Dhiman, A.K., 2010. Problem, failure and safety analysis of ammonia plant: a review. Int. Rev. Chem. Eng. 2, 631–646.
Rawlings, J.B., 2000. Tutorial overview of model predictive control. IEEE Control Syst. Mag. 20, 38–52.
Rovaglio, M., Manca, D., Cortese, F., 2004. A reliable control for the ammonia loop facing limit-cycle and snowball effects. AIChE J. 50, 1229–1241.
Shah, M.j., 1967. Control simulation in ammonia production. Ind. Eng. Chem. 59, 72–83.

Shah, M.J., Weisenfelder, A.J., 1969. Control and optimization of a large ammonia plant with a digital computer. Automatica 5, 319–333.
Twigg, M., 1989. Catalyst Handbook. Wolfe Publishing Ltd., London.
Wallace, M., Pon Kumar, S.S., Mhaskar, P., 2016. Offset-free model predictive control with explicit performance specification. Ind. Eng. Chem. Res. 55, 995–1003.
Wu, Z., Albalawi, F., Zhang, Z., Zhang, J., Durand, H., Christofides, P.D., 2018a. Model predictive control for process operational safety: utilizing safeness index-based constraints and control lyapunov-barrier functions. Comput. Aided Chem. Eng. 44, 505–510.
Wu, Z., Durand, H., Christofides, P.D., 2018b. Safeness index-based economic model predictive control of stochastic nonlinear systems. Mathematics 6, 69.
Zhang, C., Vasudevan, S., Rangaiah, G.P., 2010. Plantwide control system design and performance evaluation for ammonia synthesis process. Ind. Eng. Chem. Res. 49, 12538–12547.
Zhang, Z., Wu, Z., Durand, H., Albalawi, F., Christofides, P.D., 2018. On integration of feedback control and safety systems: analyzing two chemical process applications. Chem. Eng. Res. Des. 132, 616–626.